1-2009

Beam propagation modeling of modified volume Fresnel zone plates fabricated by femtosecond laser direct writing

Pornsak Srisungsitthisunti
Purdue University - Main Campus, psrisung@purdue.edu

Okan K. Ersoy
Purdue University - Main Campus, ersoy@purdue.edu

Xianfan Xu
Birck Nanotechnology Center, School of Materials Engineering, Purdue University, xxu@purdue.edu

Follow this and additional works at: http://docs.lib.purdue.edu/nanopub

Part of the Nanoscience and Nanotechnology Commons

Beam propagation modeling of modified volume Fresnel zone plates fabricated by femtosecond laser direct writing

Pornsak Srisungsitthisunti,[1] Okan K. Ersoy,[2,*] and Xianfan Xu[1]

[1]*School of Mechanical Engineering, Birck Nanotechnology Center, Purdue University, West Lafayette, Indiana 47907, USA*
[2]*School of Electrical and Computer Engineering, Birck Nanotechnology Center, Purdue University, West Lafayette, Indiana 47907, USA*
*Corresponding author: ersoy@ecn.purdue.edu

Light diffraction by volume Fresnel zone plates (VFZPs) is simulated by the Hankel transform beam propagation method (Hankel BPM). The method utilizes circularly symmetric geometry and small step propagation to calculate the diffracted wave fields by VFZP layers. It is shown that fast and accurate diffraction results can be obtained with the Hankel BPM. The results show an excellent agreement with the scalar diffraction theory and the experimental results. The numerical method allows more comprehensive studies of the VFZP parameters to achieve higher diffraction efficiency. © 2008 Optical Society of America

OCIS codes: 320.7110, 050.1970, 130.3120, 000.4430, 050.1960, 070.2590.

1. INTRODUCTION

The volume Fresnel zone plate (VFZP) is a focusing device consisting of a number of Fresnel zone plate (FZP) layers inside a transparent medium [1,2]. The FZPs are aligned on the same optical axis and designed to focus light to a single spot as shown in Fig. 1. By combining a number of FZPs coherently, the VFZP can achieve much higher diffraction efficiency than a conventional FZP. This is especially useful when an individual FZP can only be fabricated with small diffraction efficiency. The VFZP can be fabricated by femtosecond laser direct writing. This concept was experimentally demonstrated with an eight-layer modified VFZP, showing a maximum efficiency of 71.5% [2]. However, the performance of the VFZP is not fully optimized. The overall diffraction efficiency of the VFZP is determined by many factors such as the number of FZP layers, fabrication parameters, VFZP design, etc. The experimental study of VFZP shows that the efficiency of the VFZP continues to increase up to a certain number of FZP layers before it starts to drop [1,2]. Consequently, it is difficult to predict the diffraction efficiency of the VFZP, since light propagation by diffraction through 3D VFZP structures is complicated. A numerical simulation is necessary to study diffraction behavior of a VFZP. Understanding how light is diffracted through the VFZP will help in predicting the VFZP performance and improving the VFZP design.

Several numerical methods for diffractive optics simulation are available, including scalar diffraction theory [3], rigorous diffraction theory [4], fast Fourier transform (FFT) methods [5], beam propagation method (BPM) [6], finite element analysis (FEA) [7], finite-difference time domain method (FDTD) [8], and so on. These methods have different advantages and limitations for different simulation conditions, such as near and far fields and 1D–2D–3D calculations, which affect the accuracy of the results. In the case of the VFZP, the selected method must employ small step propagation to enable simulation of multiple diffractions through the FZP layers. The split-step BPM can handle such a situation where the field experiences

rapid modulation. In particular, the FFT-based BPM (FFT-BPM) utilizes the Fourier transform to locally decompose the entire field into plane waves that are then propagated forward in the spectral domain and corrected at each step in the spatial domain [6,9]. The FFT-based methods are preferable since they provide fast calculation with high accuracy. When circular symmetry is available, the Hankel transform (Fourier–Bessel) can be applied so that the diffraction analysis becomes 2D (r,z) instead of 3D (x,y,z) [9]. The VFZP structure has cylindrical symmetry and can utilize the Hankel transform. In this work, the Hankel transform BPM was developed to study the performance of modified VFZPs. The simulation results closely matched with the experimental results, allowing a better understanding of the influence of the VFZP design parameters.

This paper is organized as follows: the detailed description of the Hankel transform method and its implementation for VFZP are discussed in Section 2. Section 3 evaluates the accuracy of the Hankel transform results by comparison with the scalar diffraction theory. Section 4 discusses the behavior of light diffraction by a VFZP. The VFZP simulation results are discussed and compared with the experimental results in Section 5, followed by conclusions in Section 6.

Fig. 1.   (Color online) Example of a VFZP having four FZP layers.

2. LIGHT DIFFRACTION SIMULATION BY THE HANKEL TRANSFORM BEAM PROPAGATION METHOD

Wave propagation through cylindrically symmetrical structures can be simulated by using the Hankel transform and its inverse to convert back and forth between the spatial domain and the frequency domain. First, the input field is transformed to the spectral field, before propagating to the image plan by multiplying by a propagation factor, $\exp(2\pi jz\sqrt{1/\lambda^2 - (f_x^2 + f_y^2)})$. Then, the spectral field at the image plane is inverse-transformed back to the spatial field. Mathematically, the inverse Hankel transform has the same form as the Hankel transform, making the conversion process easy to implement. The Hankel transform of zero order and its inverse are given by [9,10]

$$U(\rho) = 2\pi \int_0^\infty u(r)J_0(2\pi r\rho)r\,\mathrm{d}r, \tag{1a}$$

$$u(r) = 2\pi \int_0^\infty U(\rho)J_0(2\pi r\rho)\rho\,\mathrm{d}\rho, \tag{1b}$$

where J_0 is the Bessel function of the first kind of zero order. The Hankel transform is essentially the 2D continuous Fourier transform of a circularly symmetry function.

There are several methods for the numerical calculation of the Hankel transform. A quasi-discrete Hankel transform (QDHT) developed by Guizar-Sicairos and Gutiérrez-Vega (2004) assumes a finite frequency domain and uses a transformation matrix to quickly compute the Hankel transform as well as the inverse Hankel transform [10]. The method approximates the input function by sampling at positions proportional to the positions of the zeros of a Fourier–Bessel function. In addition, the inverse Hankel transform with this method is energy preserving as it can reconstruct the original wave field. Hence, this method of Hankel transform computation prevents energy loss, and thereby is suitable for field propagation simulation. We utilized the QDHT method for the zero-order Hankel transform.

In this work, the simulation of light diffraction through the VFZP is analyzed in small steps along the propagating direction z, using the BPM method. Combined with

the Hankel transform, we refer to this method as the Hankel transform BPM (Hankel BPM). This method is also demonstrated by Guizar-Sicairos and Gutiérrez-Vega [10]. First, a VFZP is designed by generating a number of FZP layers in different axial locations. The design of each FZP layer is different, depending on its location relative to the overall focusing spot to combine light at the focus [1,2]. Then, a number of radial and axial steps are chosen, and the FZP profile at each layer is discretized with a radial step. The plane wave is converted to a spectral field and then propagated step by step in the axial direction. Only when the wave field is propagated through a FZP layer is the complex field (amplitude and phase) convolved with the FZP profile. In the simulation model, the FZPs are separated by a few propagation steps so that light interacts with one FZP layer and propagates a few steps before interacting with the next FZP layer, and so on. The wave fields are stored at each propagation step. For example, Fig. 2 shows the simulation model of a three-layer VFZP. The model is developed in the cylindrical coordinates. For simplicity, each FZP has uniform thickness and results in phase modulation within a VFZP. In addition, the radial extent of the simulation is about twice the size of the VFZP radius and the light outside the VFZP is blocked on the first layer. More importantly, to avoid aliasing from the edge of the computational window, it is necessary to apply zero padding at the edge (boundary).

In the actual fabrication, the VFZP is fabricated inside a medium such as fused silica, so light travels through two different media. A simulation can be performed by assigning the correct wavelength in fused silica ($\lambda/1.46$)—the material used for fabricating VFZP [1,2] or air during the corresponding propagation step. By applying different wavelengths, the refraction effect at fused silica and air interface is taken into account. Arbitrary phase and amplitude modulation can be introduced into the numerical model through the complex-valued trans-
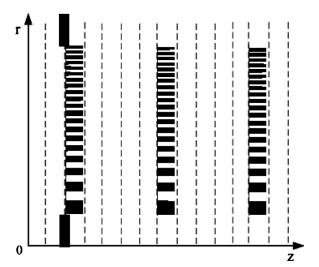

Fig. 2.   Simulation model of a three-layer VFZP showing propagation steps used by the Hankel BPM calculation. The actual computational windows are twice the size of the maximum radius.

missivity of the FZP. This allows partial phase FZP or amplitude FZP to be simulated. The Hankel BPM simulation results confirm that a phase FZP has four times the efficiency of the amplitude FZP, which agrees with the theory.

The accuracy of the Hankel BPM depends on the number of sampling steps. We concluded that the radial sampling step size should be smaller than the smallest outermost zone width to avoid nonnegligible error due to discretization. The smaller the sampling step size is, the more accurate the results that can be generated. On the other hand, using a large number of radial steps costs a significantly larger computational time. For a quick comparison, a 300-radial-step calculation took about 1.7 s on a 2.4 GHz computer with 1 Gbytes of RAM, a 1000-radial-step took 12.9 s, and a 3000-radial-step calculation took 103.3 s. As a result, we learned that 1000 radial steps were sufficient for our far-field FZP simulation. The results are much less sensitive to the number of axial steps.

The advantage of the Hankel BPM is the ease of its implementation and high numerical efficiency (i.e., computation time per propagation step is small). However, since the BPM method calculates the wave field in the forward direction, it cannot resolve the reflection wave. Since light reflection from a phase-type VFZP is negligible, this is not a major issue. Simulation allows an arbitrary VFZP design to be simulated, providing a useful prediction for the VFZP performance. Furthermore, the method can be extended to simulate noncircular structures by replacing the Hankel transform with the 2D fast Fourier transform.

3. VERIFICATION OF THE HANKEL BEAM PROPAGATION METHOD

In this section, the accuracy of the Hankel BPM method is tested by comparing its results with the results of the scalar diffraction theory. Light diffraction by a FZP can be explicitly calculated by the Rayleigh–Sommerfeld (RS) diffraction integral. Therefore, FZP diffraction by the Hankel BPM can be verified by comparing it to the RS diffraction result. The RS integral is given by [9]

$$U(P_0) = \frac{1}{j\lambda} \int \int_s U(P_1) \frac{\exp(jkr)}{r} \cos(\vec{n},\vec{r}) \mathrm{d}s. \quad (2)$$

where P_0 is a point in the observation plane, P_1 is in a point at the initial plane, $\vec{r}$ is the vector pointing from P_0 to P_1, s is the enclosed surface, $\vec{n}$ is a vector normal to the surface, k is the wave vector, and λ is the wavelength. The RS diffraction formula can evaluate the exact light field in the far field for scalar diffraction. Normally, the RS integral is difficult to solve analytically without applying the Fresnel or Fraunhofer approximation. Cao and Jahns (2004) applied the far-field $(f \gg \lambda)$ assumption, and evaluated the analytical result for FZP focusing [3]. We modified the method by Cao and Jahns [3] to simulate different types of FZPs. The RS method integrates each Fresnel ring and combines the total field intensity at the focal plane as follows:

$$U(R) = \sum_{n=1}^{N} U_n(R),$$

$$U_n(R) = \frac{1}{\lambda} \int \int_{A_n} \frac{f}{\rho^2} \exp(jk\rho) r \mathrm{d}r \mathrm{d}\theta, \quad (3)$$

where R is the radial location at the focal plane, N is the number of rings, f is the focal length of a FZP, and ρ is a function of optical path length given by $\rho = [f^2 + R^2 + r^2 - 2Rr \cos(\theta - \phi)]^{1/2}$, ϕ is the angle in the input plane, and θ is the angle in the focal plane. U_n is the focal intensity from one FZP ring and U is the total focal intensity.

As discussed in our previous work [1,2], "central-ring" FZPs were fabricated at each zone that have a uniform width and were located at the center of each Fresnel zone. The reasons are to reduce the time needed for fabrication, to make fabrication more practical with robustness against experimental errors, and to avoid zone overlapping for high numerical aperture (NA) FZPs [2]. The results of the Hankel BPM and RS integral methods are comparatively discussed for both the regular and the central-ring FZPs. The simulation geometries of the regular and central-ring FZPs are shown in Figs. 3(a) and 3(b), respectively. Both types of FZPs contain 20 Fresnel zones and have a focal length of 20 mm. The sizes of both FZPs are 1.4 mm in diameter. The results of the RS method are shown in Figs. 3(c) and 3(d). In Fig. 4, the contour plots show propagation of the light intensity by the Hankel BPM method. The gradient of the contour plots has been reduced by plotting $I^{(1/4)}$ to clearly show the propagating pattern. The axial intensity results from both methods show very similar results for the regular and central-ring FZPs. At the primary focus, the central-ring FZP has about half of the intensity of the regular FZP, because of the missing portion in each central-ring zone. Therefore, the efficiency of the central-ring FZP strongly depends on the zone width.

The appearances of the higher order foci of the two FZPs are different, and can also be used to verify the accuracy of the Hankel BPM. In the regular FZP, the foci of the even orders would cancel out completely due to symmetric counter phase shifts within one zone (destructive interference), while the foci of the odd orders remain. Therefore, the regular FZP only generates odd order foci (at $f/3, f/5, \ldots$), and the intensities of the foci decrease rapidly as the number of orders increases. On the other hand, the central-ring FZP does not fully cover the Fresnel zones, and all the orders of foci remain with some efficiency. The intensity at these higher order foci depends on the zone width of the central-ring FZP. The central-ring FZP has lower focal intensity because part of the energy goes to other higher order foci. The results suggest that both the Hankel BPM and the RS integral method correctly predict the higher order behavior as discussed previously.

In summary, for one layer FZP, the Hankel BPM method correctly predicts diffraction output of the regular and central-ring FZPs. This suggests that the Hankel BPM method is a suitable tool for FZP simulation, and is extended to VFZP simulation in this work.
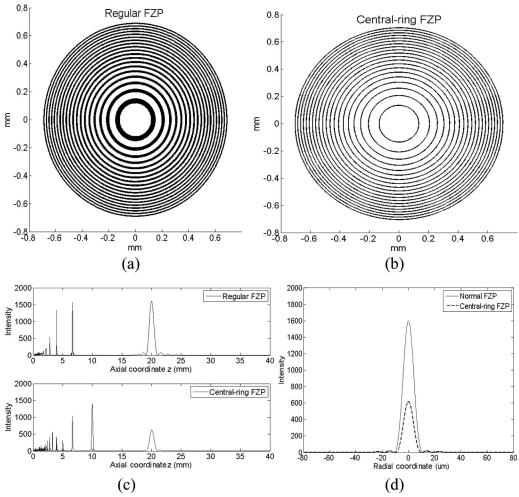
Fig. 3. (a) Regular FZP, (b) central-ring FZP, and light diffraction computed by the RS integral (c) the axial diffractions, (d) the radial diffractions at the focal plane.

4. DIFFRACTION ANALYSIS OF VOLUME FRESNEL ZONE PLATE

In this section the Hankel BPM is used to study diffraction by a VFZP (see Fig. 5). For the simplest case of a two-layer VFZP, diffraction of light can be separated into three beams as shown in Fig. 6. The first and second beams are due to single diffraction by FZP1 and FZP2, and they are combined at the focus spot as designed. The third beam is a result of the first beam diffracted again by the FZP2, and projected to another spot at a shorter distance than the focal length. This is equivalent to the focusing of a compound lens. A simple calculation using geometrical optics can determine the location of the focusing spot of the third beam. This location depends on the separation of the two FZPs. The Hankel BPM simulation is expected to calculate all the diffractions including the light spot due to multiple diffractions. Therefore, simulations of single layer and two-layer central-ring VFZPs are performed in order to compare the intensity of the primary focus and the extra focusing spot. The simulation results are shown in Fig. 6. While the intensity at the primary focus of the two-layer VFZP doubles, the higher order foci intensities are slightly decreased. This is because the VFZP is designed for a phase matching condition at the primary focus only. In addition, the simulation result

clearly identified the spot due to double diffraction at the location as calculated by the compound lens focusing method. We conclude that diffraction by the VFZP consists of primary diffractions, and multiple diffractions and the Hankel BPM simulated all the diffracted light correctly.

The spots created by multiple diffractions usually have low efficiency. For example, if each FZP has 10% efficiency, the efficiency becomes 1% by double focusing. Thus, for a VFZP consisting of a larger number of FZP layers, focusing due to multiple diffractions is negligible.

5. VOLUME FRESNEL ZONE PLATE SIMULATIONS

A major purpose of VFZP simulation is to study how the efficiency increase is associated with the number of FZP layers and the amount of phase modulation applied at each FZP layer. Diffraction efficiency can be calculated by dividing the focal energy by the total input energy. Normally, the size of the focus is defined as $\omega_0 = 0.61\lambda/NA$, where NA is the numerical aperture of the VFZP. Therefore, the diffraction efficiency is given by
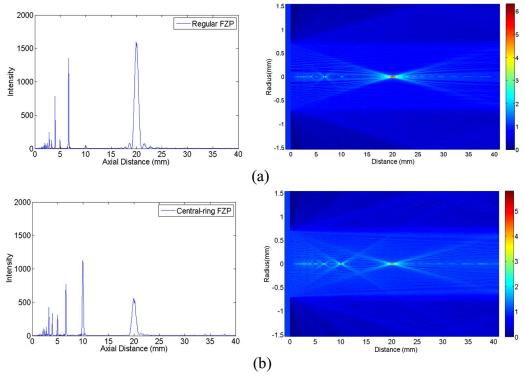
Fig. 4.   (Color online) Diffraction results calculated by Hankel BPM for (a) the regular FZP and (b) the central-ring FZP. The gradient of the contour plots was reduced by plotting $I^{(1/4)}$ to clearly show the propagating pattern.

$$\eta = \frac{I_{\omega_0}}{I_{\text{input}}} = \frac{\int_0^{\omega_0} I \, dr}{\int_0^{\text{aperture}} I \, dr}. \qquad (4)$$

The regular VFZP and the central-ring VFZP designed for 20 mm focal length, consisting of up to 20 FZP layers, were simulated. These VFZPs are assumed to have uniform phase modulation at each FZP layer from 0.05π to 0.4π. Figures 7 and 8 show the relationship of the phase modulation and the number of FZP layers on the diffraction efficiencies of the regular and central-ring VFZP, respectively. Clearly, the number of layers that produces maximum diffraction efficiency of a VFZP depends on the phase modulation of each individual FZP. The lower the
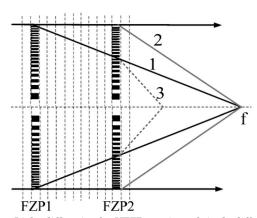

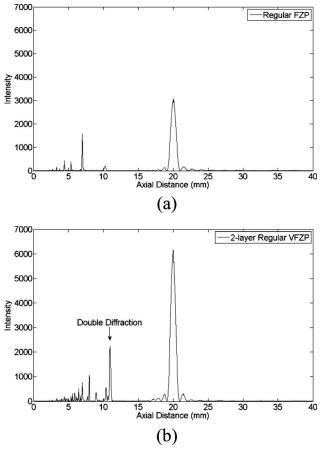Fig. 5.   Light diffraction by VFZP consists of single diffractions (1,2) and multiple diffractions (3).

Fig. 6.   Comparison of (a) the regular FZP and (b) the two-layer regular VFZP to show the effect of double diffraction by the Hankel BPM. The phase modulation is 0.5π for each FZP layer.
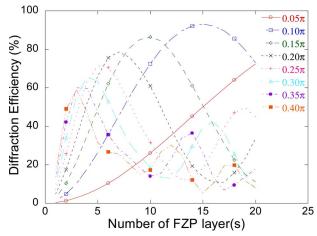
Fig. 7. (Color online) Simulation of regular VFZPs having up to 20 layers with phase modulations from 0.05π to 0.4π.

phase modulation, the higher the number of layers required to reach the maximum efficiency. For example, in the regular VFZP case, the small phase shift of 0.05π requires more than 20 layers, while the phase shift of 0.4π requires only 4–5 layers to reach maximum diffraction efficiency. In general, the regular VFZP requires less number of FZP layers to achieve maximum possible efficiency, since each regular FZP has higher efficiency than the corresponding central-ring FZP. Once the efficiency reaches the maximum, more layers of FZP causes efficiency to drop. Small phase modulation tends to achieve higher overall diffraction efficiency. Therefore, the VFZP is an effective method in terms of improving efficiency when the individual FZP is limited to small efficiency. A major conclusion is that it is possible to achieve high diffraction efficiency with the central-ring VFZP close to that of the regular VFZP, and much higher than single regular FZP. This central-ring VFZP method is competitive with multilevel phase FZP, yet has the advantage of easy implementation, for example, within glass volume media. Although the regular VFZP can reach a little higher efficiency, the fabrication time is much higher than the central-ring VFZP, and is much more sensitive to fabrication errors. It is worth mentioning that the full width at
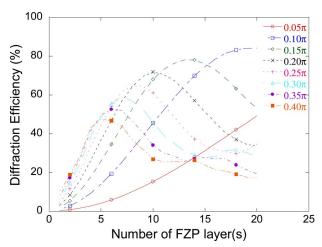
half-maximum (FWHM) of the central-ring VFZP is comparable to the FWHM of the regular VFZP. This indicates that the focal spot size is a function of the NA, and the central-ring VFZP can be used for high resolution focusing.

The central-ring VFZP simulations also yield the following results, which are helpful for the design of the VFZP:

• The amount of phase modulation is directly related to individual FZP efficiency. The smaller the FZP efficiency, the higher the VFZP efficiency can reach. However, it is not practical to use more than 20 layers to get slightly higher efficiency.

• Increasing the number of zones improves the individual FZP efficiency since a larger amount of light is diffracted, and it requires fewer FZP layers to achieve maximum VFZP efficiency. The effect of the number of zones is similar to the effect of phase modulation.

• The focal length has an interesting effect. In Fig. 9, central-ring VFZPs with different focal lengths were simulated at a constant phase modulation of 0.23π. The results suggest that the efficiency for the single layer FZP is higher for the shorter focal length, but the overall VFZP efficiency is highest for the 10 mm focal length. This can be explained since the zone width is constant and optimized for the design of the shorter focal length in the experiments. A longer focal length would require wider center rings. However, the optimized zone width for FZP is different for VFZP, and the 10 mm focal length VFZP appears to be more efficient.

• The zone width of the central-ring FZP should be about the size of the average regular zone. A too wide or too narrow zone induces more phase error and reduces the individual efficiency.

• The separation distance between FZPs has negligible effect on the results. The exception is the case of the separation distance approaching zero; the efficiency only improves for the first few FZP layers and is limited to a small overall efficiency.

Next, the simulation results are compared with the experimental results. The central-ring VFZPs were fabri-
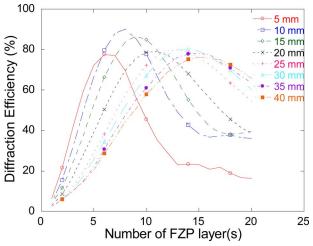

Fig. 8. (Color online) Simulation of central-ring VFZPs having up to 20 layers with phase modulations from 0.05π to 0.4π.

Fig. 9. (Color online) Simulation of central-ring VFZPs having up to 20 layers with different focal lengths and constant phase modulation of 0.23π.
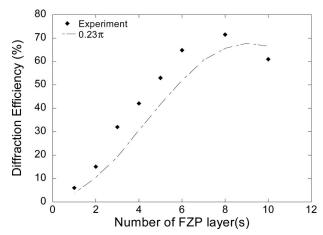
Fig. 10. Comparison of the experimental results and the simulation results for the central-ring VFZP having 0.23π phase modulation.

cated with a different number of layers up to 10 layers in fused silica by femtosecond laser direct writing. The details of the experiments are explained in [2]. The actual phase modulation induced by each FZP is the amount of refractive index change multiplied by the thickness of the FZP layer, which depends on the laser power, scanning speed, focusing lens, and depth of fabrication. Our fabricated FZP was 250 μm thick and had a refractive index change of 0.2×10^{-3}. The refractive index was estimated by the grating fabrication method [2]. As a result, the actual phase shift was approximately $\phi = 2\pi \cdot (\text{thick}) \cdot (\Delta n)/(\lambda/n) = 0.23\pi$. Therefore, the central-ring VFZP simulation having a phase shift of 0.23π as measured in the experiments was used in the simulation. Figure 10 compares simulation results for the central-ring VFZP having a phase modulation of 0.23π with the experimental results under the same conditions. The phase modulation of 0.23π has maximum efficiency at nine layers, whereas the experimental result showed maximum efficiency at eight layers. Normally, we would expect the measured efficiencies to be lower than the simulated efficiencies due to fabrication errors, etc. However, the calculated results from the Hankel BPM appear to be lower than the experimental results. This is possibly due to the measurement setup in which the intensity of the spot was measured through a pinhole that was larger than the FWHM of the focal spot. As a result, the measured efficiency is overestimated by about 5%–10%. Nevertheless, the Hankel BPM accurately predicts the behavior of the efficiency increase by VFZPs and can be used for the simulation of other 3D circularly symmetric diffractive optical devices.

6. CONCLUSIONS

In this paper, we present an accurate and efficient numerical method for simulation of focusing by VFZPs. The Hankel BPM simulation results were confirmed by the Rayleigh–Summerfield integral method for the amplitude FZPs. The Hankel BPM provides useful comparison of diffraction by regular and central ring VFZPs. The central-ring VFZP has advantages in fast fabrication and robustness against fabrication errors, and can achieve nearly as high a diffraction efficiency as the regular VFZP. The numerical method allows for the investigation of VFZP parameters including phase modulation, number of FZP layers, focal length, number of rings, etc. Furthermore, the efficiency simulation results with the VFZP matches the experimental results reasonably well. The results suggest that the phase modulation by each individual FZP determines the number of FZP layers required to achieve maximum efficiency. The maximum diffraction efficiency is sensitive to several parameters used in the design of the VFZP. As a result, the numerical simulation approach was successfully developed to predict the diffraction output of the VFZP as a function of these parameters. Our future work will be using the Hankel BPM to design and fabricate a more efficient VFZP.

ACKNOWLEDGMENTS

REFERENCES

1. P. Srisungsitthisunti, O. K. Ersoy, and X. Xu, "Volume Fresnel zone plates fabricated by femtosecond laser direct writing," Appl. Phys. Lett. **90**, 011104 (2007).
2. P. Srisungsitthisunti, O. K. Ersoy, and X. Xu, "Laser direct writing of volume modified Fresnel zone plates," J. Opt. Soc. Am. B **24**, 2090–2096 (2007).
3. Q. Cao and J. Jahns, "Comprehensive focusing analysis of various Fresnel zone plates," J. Opt. Soc. Am. A **21**, 561–571 (2004).
4. D. M. Chambers and G. P. Nordin, "Stratified volume diffractive optical elements as high-efficiency gratings," J. Opt. Soc. Am. A **16**, 1184–1193 (1999).
5. F. Wyrowski, "Diffractive optical elements: iterative calculation of quantized, blazed phase structures," J. Opt. Soc. Am. A **7**, 961–969 (1990).
6. R. Piestun and J. Shamir, "Control of wave-front propagation with diffractive elements," Opt. Lett. **19**, 771–773 (1994).
7. A. N. Kurokhtin and A. V. Popov, "Simulation of high-resolution x-ray zone plates," J. Opt. Soc. Am. A **19**, 315–324 (2002).
8. D. W. Prather and S. Shi, "Formulation and application of the finite-difference time-domain method for the analysis of axially symmetric diffractive optical elements," J. Opt. Soc. Am. A **16**, 1131–1142 (1999).
9. O. K. Ersoy, *Diffraction, Fourier Optics and Imaging* (Wiley-Interscience, 2006), pp. 21, 57–58, 190–191.
10. M. Guizar-Sicairos and J. Gutiérrez-Vega, "Computation of quasi-discrete Hankel transforms of integer order for propagating optical wave fields," J. Opt. Soc. Am. A **21**, 53–58 (2004).